

The BigApple force and its implications to finite nuclei and astrophysical objects

H. C. Das^{1,2,*}, Ankit Kumar^{1,2,†}, Bharat Kumar³, S. K. Biswal⁵, and S. K. Patra^{1,2}

¹*Institute of Physics, Sachivalaya Marg, Bhubaneswar-751005, India*

²*Homi Bhabha National Institute, Training School Complex, Anushakti Nagar, Mumbai 400094, India*

³*Department of Physics & Astronomy, National Institute of Technology, Rourkela, India* and

⁵*Department of Astronomy, Xiamen University, Xiamen 361005, P. R. China*

(Dated: September 23, 2020)

The mass gap in the secondary component of the GW190814 event left us, “whether it is a super-massive neutron star or light black-hole?”. Recently, Fattoyev *et al.* have predicted the mass of the secondary component is $2.60 M_{\odot}$ based on the BigApple parameter set. We study the properties of finite nuclei, nuclear matter and neutron star by using the BigApple parameter set along with four well-known relativistic mean-field forces namely NL3, G3, IOPB-I and FSUGarnet. The predicted nuclear properties like binding energy per particle, skin thickness, charge radius, single-particle energy and two-neutron separation energy are well satisfied by the BigApple for a series of nuclei. The calculated nuclear matter quantities such as incompressibility, symmetry energy and its slope parameters are consistent with the empirical/experimental values available till date. The canonical tidal deformability of the BigApple is well suited by the GW190814 data. The dimensionless moment of inertia lies in the range given by the analysis of PSR J0737-3039A. In spite of all the success, the equation of state produced by the BigApple doesn’t follow the flow data and suggest a refitting of the force parameters along with the additional coupling terms.

I. INTRODUCTION

The detection of gravitational wave (GW) from the two neutron stars (NSs) merger event GW170817 [1, 2] by the LIGO and Virgo collaboration (LVC) provides us the opportunity to study the properties of dense matter at extreme conditions. Further, with the recent discovery event GW190814, the LVC detected the collision of a black hole of mass $22.2\text{--}24.3 M_{\odot}$ with a compact object of mass $2.50\text{--}2.67 M_{\odot}$ [3]. The secondary component of GW190814 has no measurable signature of tidal deformability, and also there is no electromagnetic counterpart on the gravitational waveform. This left us doubt, and arises the question, “whether the secondary component of GW190814 is either a massive NS or lightest black hole?”.

The GW190814 event opens the possibility to achieve the super-massive NS only when the equation of state (EoS) is very stiff. That EoS can be constructed by using various effective theory approaches, like relativistic mean-field (RMF) formalism [4–9], Skyrme-Hartree-Fock (SHF) [10–13], Density-dependent RMF (DDRMF) [14–17] etc. The recent works [18–24] have been dedicated to explore the secondary component of GW190814. Tan *et al.* [25] considered that it may be a heavy NS with deconfined QCD core. In the Ref. [26], they assumed that it may be a super-fast pulsar. Recently, Fattoyev and collaborators [27] assumed it to be a binary black-hole merger which is supported by Tews *et al.* [20]. Using the DDRMF model in Ref. [24], it is reported that there is a possibility of the secondary component in GW190814 as NS. The maximum mass of the MSP J0740+6620 is $2.14^{+0.10}_{-0.09} M_{\odot}$ with 68.3% credible limit, which is considered to be the heaviest NS till date [28]. Also, in Ref. [29], the upper limit of the NS mass is constraint to $M_{max} \lesssim 2.17 M_{\odot}$ (90%) which

is consistent with Cromartie *et al.* [28]. However, one can not exclude the existence of the super-massive NS in the secondary component of GW190814.

From the last four decades, a large number of energy density functionals (EDFs) have been formed to study the properties of finite nuclei and infinite nuclear matter. In a recent review by Dutra *et al.* [13, 30] noticed that only a few EDFs forces which can consistently reproduce the properties of the finite nuclei, nuclear matter (NM) and the NS. To form a super-massive NS with a mass range $2.50\text{--}2.67 M_{\odot}$ is not a big deal but to reconcile the super-massive NS with different properties of finite/infinite nuclear systems is quite difficult. The GW170817 has been put a limit on the tidal deformability of the canonical NS, which is used to constraint the EoS of neutron-rich matter at 2-3 times of the nuclear saturation densities [1]. Due to a strong dependence of tidal deformability with radius ($\Lambda \sim R^5$), it can put a stringent constraints on the EoS. Several approaches [31–39] have been tried to constraint the EoS on the tidal deformability bound by the GW170817. In particular, the GW170817 favours a star with relatively smaller radius, which needs a soft EoS. These constraints are also consistent with the recent determination of mass-radius by the *Neutron star Interior Composition Explorer* (NICER) with X-ray study of the millisecond pulsar PSR J0030+0451. [40–43].

The tension is to reconcile the prediction of super-massive NS, which requires stiff EoS and the soft EoS demanded by the GW170817 and NICER observation. Fattoyev *et al.* have been tried to reconcile the two facts which are based on the density functional theory. They have predicted the NS maximum mass as $2.60 M_{\odot}$ from the covariant EDFs, which is named as ‘BigApple’ [27]. Here, we briefly describe the formalism of the BigApple EDF. The parameters ζ and Λ_V play a significant role in the formation of stiff EoS of the NM. In BigApple EDF, the value of ζ is tuned in such a way, which predicts the mass of the NS as $2.60 M_{\odot}$. To reproduce the other NM parameters, they have slightly changed the slope

* harishdas.physics@gmail.com

† ankit.k@iopb.res.in

of the symmetry energy which predicts the skin thickness of ^{208}Pb as 0.15 fm. The binding energies, charge radii of ^{40}Ca and ^{208}Pb have been fixed by the re-adjusting the mass of the σ -meson, the NM saturation density and the binding energy at the saturation. The detailed prescription is given in [27]. In present paper, we systematically study the BigApple EDF from finite nuclei to the NS.

The BigApple parameter set predict not only the finite nuclei properties like binding energy per nucleon, charge radius and skin thickness for a series of nuclei but also the NM parameters as well. But the EoS of BigApple doesn't satisfy the heavy-ion data. The predicted dimensionless tidal deformability by BigApple also doesn't look consistent with GW170817 due to its stiffer EoS. The calculated canonical radius lies in the range given by the NICER. Therefore, to predict the properties ranging from finite nuclei to NS, the EoS must consistent with the flow data, which requires a tuning of the parameters of the BigApple parameter set along with the addition of other couplings.

The paper is organised as follows: the formalism used in this work is given in Section II. In Sub-Section II A, we de-

scribe the basic formalism of RMF approach using BigApple along with other four parameter sets. In Sub-Section II B, we calculate the NM properties such as EoS, incompressibility, symmetry energy and its different coefficients etc. for five known parameter sets. We present the results and discussion in Section III, which includes finite nuclei, NM and NS in detail. Finally, we give concluding remarks in Section IV.

II. FORMALISM

A. Energy density functional

In RMF prescription, the nucleons interact with each other through exchange of different mesons like σ , ω , ρ and δ . We form a model which include all possible interactions for nucleon-mesons and their self and cross interactions up to fourth order known as the effective field theory motivated relativistic mean-field (E-RMF). The parameters used in the E-RMF formalism are fitted to reproduce the observables of finite nuclei and infinite NM. The E-RMF Lagrangian is given in Refs. [5, 8, 9, 44]:

$$\begin{aligned} \mathcal{E}(r) = & \sum_{\alpha=p,n} \varphi_{\alpha}^{\dagger}(r) \left\{ -i\boldsymbol{\alpha} \cdot \boldsymbol{\nabla} + \beta \left[M - \Phi(r) - \tau_3 D(r) \right] + W(r) + \frac{1}{2} \tau_3 R(r) + \frac{1 + \tau_3}{2} A(r) - \frac{i\beta\boldsymbol{\alpha}}{2M} \cdot \left(f_{\omega} \boldsymbol{\nabla} W(r) \right. \right. \\ & \left. \left. + \frac{1}{2} f_{\rho} \tau_3 \boldsymbol{\nabla} R(r) \right) \right\} \varphi_{\alpha}(r) + \left(\frac{1}{2} + \frac{\kappa_3}{3!} \frac{\Phi(r)}{M} + \frac{\kappa_4}{4!} \frac{\Phi^2(r)}{M^2} \right) \frac{m_s^2}{g_s^2} \Phi^2(r) - \frac{\zeta_0}{4!} \frac{1}{g_{\omega}^2} W^4(r) + \frac{1}{2g_s^2} \left(1 + \alpha_1 \frac{\Phi(r)}{M} \right) \left(\boldsymbol{\nabla} \Phi(r) \right)^2 \\ & - \frac{1}{2g_{\omega}^2} \left(1 + \alpha_2 \frac{\Phi(r)}{M} \right) \left(\boldsymbol{\nabla} W(r) \right)^2 - \frac{1}{2} \left(1 + \eta_1 \frac{\Phi(r)}{M} + \frac{\eta_2}{2} \frac{\Phi^2(r)}{M^2} \right) \frac{m_{\omega}^2}{g_{\omega}^2} W^2(r) - \frac{1}{2e^2} \left(\boldsymbol{\nabla} A(r) \right)^2 - \frac{1}{2g_{\rho}^2} \left(\boldsymbol{\nabla} R(r) \right)^2 \\ & - \frac{1}{2} \left(1 + \eta_{\rho} \frac{\Phi(r)}{M} \right) \frac{m_{\rho}^2}{g_{\rho}^2} R^2(r) - \Lambda_{\omega} \left(R^2(r) \times W^2(r) \right) + \frac{1}{2g_{\delta}^2} \left(\boldsymbol{\nabla} D(r) \right)^2 + \frac{1}{2} \frac{m_{\delta}^2}{g_{\delta}^2} D^2(r), \end{aligned} \quad (1)$$

where Φ , W , R and D are the redefined fields $\Phi = g_s \sigma$, $W = g_{\omega} \omega$, $R = g_{\rho} \vec{\rho}$ and $D = g_{\delta} \delta$. The coupling constants g_{σ} , g_{ω} , g_{ρ} , g_{δ} , and the masses m_{σ} , m_{ω} , m_{ρ} and m_{δ} respectively given for σ , ω , ρ , and δ mesons. $\frac{e^2}{4\pi}$ is the photon coupling constant. The coupling constants and masses for different mesons are listed in Table I for five different parameter sets (NL3 [4], FSUGarnet [45], G3 [8], IOPB-I [9] and BigApple [27]).

From the E-RMF Lagrangian in Eq.1, we get the equation of motions for the considered mesons and nucleons fields using the equation $(\partial\mathcal{E}/\partial\phi_i)=0$ for the constant density. The field equations are solved by self-consistently to get all the mesons fields. The single particle energy for the nucleon is obtained by the energy eigenvalue of the Dirac equation. The wave function $\varphi_{\alpha}(r)$ becomes

$$\frac{\partial}{\partial\varphi_{\alpha}^{\dagger}(r)} \left[\mathcal{E}(r) - \sum_{\alpha} \varphi_{\alpha}^{\dagger}(r) \varphi_{\alpha}(r) \right] = 0, \quad (2)$$

$$\begin{aligned} & \left\{ -i\boldsymbol{\alpha} \cdot \boldsymbol{\nabla} + \beta \left[M - \Phi(r) - \tau_3 D(r) \right] + W(r) + \frac{1}{2} \tau_3 R(r) \right. \\ & \left. + \frac{1 + \tau_3}{2} A(r) - \frac{i\beta\boldsymbol{\alpha}}{2M} \cdot \left[f_{\omega} \boldsymbol{\nabla} W(r) + \frac{1}{2} f_{\rho} \tau_3 \boldsymbol{\nabla} R(r) \right] \right\} \varphi_{\alpha}(r) \\ & = \varepsilon_{\alpha} \varphi_{\alpha}(r). \end{aligned} \quad (3)$$

The mean-field equations for Φ , W , R , D and A are given by

$$\begin{aligned} -\Delta\Phi(r) + m_s^2\Phi(r) = & g_s^2\rho_s(r) - \frac{m_s^2}{M}\Phi^2(r) \left(\frac{\kappa_3}{2} + \frac{\kappa_4}{3!} \frac{\Phi(r)}{M} \right) \\ & + \frac{g_s^2}{2M} \left(\eta_1 + \eta_2 \frac{\Phi(r)}{M} \right) \frac{m_{\omega}^2}{g_{\omega}^2} W^2(r) + \frac{\eta_{\rho}}{2M} \frac{g_s^2}{g_{\rho}^2} m_{\rho}^2 R^2(r) \\ & + \frac{\alpha_1}{2M} [(\boldsymbol{\nabla}\Phi(r))^2 + 2\Phi(r)\Delta\Phi(r)] + \frac{\alpha_2}{2M} \frac{g_s^2}{g_{\omega}^2} (\boldsymbol{\nabla}W(r))^2, \end{aligned} \quad (4)$$

$$\begin{aligned}
& -\Delta W(r) + m_\omega^2 W(r) = g_\omega^2 \left(\rho(r) + \frac{f_\omega}{2} \rho_T(r) \right) - \frac{1}{3!} \zeta_0 W^3(r) \\
& - \left(\eta_1 + \frac{\eta_2}{2} \frac{\Phi(r)}{M} \right) \frac{\Phi(r)}{M} m_\omega^2 W(r) - 2\Lambda_\omega g_\omega^2 R^2(r) W(r) \\
& + \frac{\alpha_2}{M} \left[\nabla \Phi(r) \cdot \nabla W(r) + \Phi(r) \Delta W(r) \right], \quad (5)
\end{aligned}$$

$$\begin{aligned}
& -\Delta R(r) + m_\rho^2 R(r) = \frac{1}{2} g_\rho^2 \left(\rho_3(r) + \frac{1}{2} f_\rho \rho_{T,3}(r) \right) \\
& - \eta_\rho \frac{\Phi(r)}{M} m_\rho^2 R(r) - 2\Lambda_\omega g_\rho^2 R(r) W^2(r), \quad (6)
\end{aligned}$$

$$-\Delta D(r) + m_\delta^2 D(r) = g_\delta^2 \rho_{s3}, \quad (7)$$

$$-\Delta A(r) = e^2 \rho_p(r). \quad (8)$$

The baryon ρ_b , scalar ρ_s , iso-vector ρ_3 , iso-scalar ρ_{s3} , charge ρ_p , tensor ρ_t and iso-tensor densities $\rho_{t,3}$ are given as follow

$$\begin{aligned}
\rho_b(r) &= \sum_{\alpha=p,n} \varphi_\alpha^\dagger(r) \varphi_\alpha(r) = \rho_p(r) + \rho_n(r) \\
&= \sum_{\alpha=p,n} \frac{2}{(2\pi)^3} \int_0^{k_\alpha} d^3k, \quad (9)
\end{aligned}$$

$$\begin{aligned}
\rho_s(r) &= \sum_{\alpha=p,n} \varphi_\alpha^\dagger(r) \beta \varphi_\alpha(r) = \rho_{sp}(r) + \rho_{sn}(r) \\
&= \sum_{\alpha=p,n} \frac{2}{(2\pi)^3} \int_0^{k_\alpha} d^3k \frac{M_\alpha^*}{(k_\alpha^2 + M_\alpha^{*2})^{\frac{1}{2}}}, \quad (10)
\end{aligned}$$

$$\rho_3(r) = \sum_{\alpha=p,n} \varphi_\alpha^\dagger(r) \tau_3 \varphi_\alpha(r) = \rho_p(r) - \rho_n(r), \quad (11)$$

$$\rho_{s3}(r) = \sum_{\alpha=p,n} \varphi_\alpha^\dagger(r) \tau_3 \beta \varphi_\alpha(r) = \rho_{ps}(r) - \rho_{ns}(r), \quad (12)$$

$$\rho_p(r) = \sum_{\alpha=p,n} \varphi_\alpha^\dagger(r) \left(\frac{1 + \tau_3}{2} \right) \varphi_\alpha(r), \quad (13)$$

$$\rho_t(r) = \sum_{\alpha=p,n} \frac{i}{M} \nabla \cdot [\varphi_\alpha^\dagger(r) \beta \boldsymbol{\alpha} \varphi_\alpha(r)], \quad (14)$$

and

$$\rho_{t,3}(r) = \sum_{\alpha} \frac{i}{M} \nabla \cdot [\varphi_\alpha^\dagger(r) \beta \boldsymbol{\alpha} \tau_3 \varphi_\alpha(r)]. \quad (15)$$

Here k_α is the Fermi momentum of the nucleon and the summation is over all the occupied states.

The parameters are obtained by fitting the data for few spherically known nuclei (^{16}O , ^{40}Ca , ^{48}Ca , ^{68}Ni , ^{90}Zr , $^{100,132}\text{Sn}$ and ^{208}Pb) along with the heavy-ion collision (HIC) data. The empirical NM properties such as binding energy per

particle, density at saturation and incompressibility are calculated using the obtained parameter sets, whose values are given in Table II. The ground-state properties of finite/infinite nuclear systems are obtained numerically in a self-consistent iterative method. The total binding energy of the nucleus is written as

$$\begin{aligned}
E_{total} &= E_{part} + E_\sigma + E_\omega + E_\rho + E_\delta \\
&+ E_c + E_{pair} + E_{c.m.}, \quad (16)
\end{aligned}$$

where E_{part} is the sum of the single-particle energies of the nucleons and E_σ , E_ω , E_ρ , E_δ are the energies of the respective mesons. E_c is the energy from the Columbic repulsion due to protons. $E_{c.m.} = 41A^{-1/3}$ is the centre of mass energy correction evaluated with a non-relativistic approximation [46, 47]. The pairing energy E_{pair} is calculated by assuming few quasi-particle level as developed in Refs. [9, 48]. Here, we take the pairing between proton-proton and neutron-neutron, which are invariant under time-reversal symmetry. The pairing can not be ignored for nuclei near to drip line because they have quasi-particles states near the Fermi surface. The simple BCS approximation is appropriate for nuclei near to the stability line. [49, 50]. However, it breaks down near the drip line. This is because the Fermi level approaches to zero, and the number of available states above the Fermi surface will decrease. For this case, the particle-hole and pair excitations to reach the continuum and their wave functions are not localised in a region, which gives rise to unphysical neutron and proton gas around the nucleus. To overcome this situation, one has to take the BCS calculations with quasi-particle states to take care of the pairing interaction [51].

To deal with pairing contribution, we use a simple approach which is found successful in Refs. [47, 48] to explain both β -stable and β -unstable nuclei. This method is similar to the prescription adopted by Chabanat *et al.* [52]. A constant pairing matrix element G_q is assumed for each kind of nucleons which gives the zero range pairing force. On top of it, we include few quasi-bound levels in the BCS calculations [47, 48, 53]. These quasi-bound states are generated by the centrifugal barrier for neutrons and centrifugal plus Coulomb for protons, which mock up the continuum states in the correlations. These wave functions of the quasi-bound states are generally localized in the classical allowed region and sharply decreases outside it. As a result, the contribution of the unphysical nucleons gas surrounding the nucleus eliminated from the BCS calculations [54]. In our calculation, we take one harmonic oscillator shell both above and below the Fermi surface. A detail description of the method is given in Refs. [47, 48, 53]

B. Nuclear Matter Properties

1. The equation of state of the NM

To find out the NM properties, one has to switched-off the electromagnetic part, surface part and also the gradient terms in the field Eqs. (4-8). The energy density and pressure for the

NM system is calculated using the energy-momentum tensor technique [55], which are given as [9, 56].

$$\begin{aligned} \mathcal{E} = & \frac{\gamma}{(2\pi)^3} \sum_{\alpha=p,n} \int_0^{k_\alpha} d^3k E_\alpha^*(k_\alpha) + \rho_b W + \frac{1}{2} \rho_3 R \\ & + \frac{m_s^2 \Phi^2}{g_s^2} \left(\frac{1}{2} + \frac{\kappa_3}{3!} \frac{\Phi}{M} + \frac{\kappa_4}{4!} \frac{\Phi^2}{M^2} \right) - \frac{1}{4!} \frac{\zeta_0 W^4}{g_\omega^2} \\ & - \frac{1}{2} m_\omega^2 \frac{W^2}{g_\omega^2} \left(1 + \eta_1 \frac{\Phi}{M} + \frac{\eta_2}{2} \frac{\Phi^2}{M^2} \right) \\ & - \Lambda_\omega (R^2 \times W^2) - \frac{1}{2} \left(1 + \frac{\eta_\rho \Phi}{M} \right) \frac{m_\rho^2}{g_\rho^2} R^2 \\ & + \frac{1}{2} \frac{m_\delta^2}{g_\delta^2} D^2, \end{aligned} \quad (17)$$

and

$$\begin{aligned} P = & \frac{\gamma}{3(2\pi)^3} \sum_{\alpha=p,n} \int_0^{k_\alpha} d^3k \frac{k^2}{E_\alpha^*(k_\alpha)} + \frac{1}{4!} \frac{\zeta_0 W^4}{g_\omega^2} \\ & - \frac{m_s^2 \Phi^2}{g_s^2} \left(\frac{1}{2} + \frac{\kappa_3}{3!} \frac{\Phi}{M} + \frac{\kappa_4}{4!} \frac{\Phi^2}{M^2} \right) \\ & + \frac{1}{2} m_\omega^2 \frac{W^2}{g_\omega^2} \left(1 + \eta_1 \frac{\Phi}{M} + \frac{\eta_2}{2} \frac{\Phi^2}{M^2} \right) \\ & + \Lambda_\omega (R^2 \times W^2) + \frac{1}{2} \left(1 + \frac{\eta_\rho \Phi}{M} \right) \frac{m_\rho^2}{g_\rho^2} R^2 \\ & - \frac{1}{2} \frac{m_\delta^2}{g_\delta^2} D^2. \end{aligned} \quad (18)$$

The $E_\alpha^*(k_\alpha) = \sqrt{k_\alpha^2 + M_\alpha^{*2}}$, where k_α is the momentum and γ is the spin degeneracy factor which is equal to 2 for individual nucleons. The M_α^* is the effective masses of nucleon given as

$$M_{p,n}^* = M + \Phi \mp D. \quad (19)$$

2. Symmetry energy and its different co-efficients

The energy density \mathcal{E} can be expanded in a Taylor series in terms of asymmetry factor $\xi (= \frac{\rho_n - \rho_p}{\rho_n + \rho_p})$ [9, 57, 58].

$$\mathcal{E}(\rho, \xi) = \mathcal{E}(\rho, \xi = 0) + S(\rho) \xi^2 + \mathcal{O}(\xi^4), \quad (20)$$

where $\mathcal{E}(\rho, \xi = 0)$ is the energy of symmetric NM, ρ is the baryonic density and $S(\rho)$ is the symmetry energy, which is defined as

$$S(\rho) = \frac{1}{2} \left(\frac{\partial^2 \mathcal{E}}{\partial \xi^2} \right)_{\xi=0}. \quad (21)$$

The density dependence symmetry energy is the most uncertain properties of the NM. A lot of progress have been made

TABLE I. The NM parameters for NL3 [4], FSUGarnet [45], G3 [8], IOPB-I [9] and BigApple [27] are listed. The mass of nucleon M is 939 MeV. The dimension of k_3 is fm^{-1} and all other coupling constants are dimensionless.

Parameter	NL3	FSUGarnet	G3	IOPB-I	BigApple
m_s/M	0.541	0.529	0.559	0.533	0.525
m_ω/M	0.833	0.833	0.832	0.833	0.833
m_ρ/M	0.812	0.812	0.820	0.812	0.812
m_δ/M	0.0	0.0	1.043	0.0	0.0
$g_s/4\pi$	0.813	0.837	0.782	0.827	0.769
$g_\omega/4\pi$	1.024	1.091	0.923	1.062	0.980
$g_\rho/4\pi$	0.712	1.105	0.962	0.885	1.126
$g_\delta/4\pi$	0.0	0.0	0.160	0.0	0.0
k_3	1.465	1.368	2.606	1.496	1.878
k_4	-5.688	-1.397	1.694	-2.932	-7.382
ζ_0	0.0	4.410	1.010	3.103	0.106
η_1	0.0	0.0	0.424	0.0	0.0
η_2	0.0	0.0	0.114	0.0	0.0
η_ρ	0.0	0.0	0.645	0.0	0.0
Λ_ω	0.0	0.043	0.038	0.024	0.047
α_1	0.0	0.0	2.000	0.0	0.0
α_2	0.0	0.0	-1.468	0.0	0.0
$f_\omega/4$	0.0	0.0	0.220	0.0	0.0
$f_\rho/4$	0.0	0.0	1.239	0.0	0.0
β_σ	0.0	0.0	-0.087	0.0	0.0
β_ω	0.0	0.0	-0.484	0.0	0.0

both experimentally and theoretically to constrain the $S(\rho)$ at different densities limit varies from heavy-ion collision experiments to NS [59, 60]. It has a large diversion at high-density limit that depends on the model used [61]. Here, we can expand the $S(\rho)$ in a leptodermous expansion near the saturation density. The expression of density dependence symmetry energy is as follow [9, 47, 62–64]:

$$S(\rho) = J + L\eta + \frac{1}{2} K_{sym} \eta^2 + \frac{1}{6} Q_{sym} \eta^3 + \mathcal{O}(\eta^4), \quad (22)$$

where $\eta = \frac{\rho - \rho_0}{3\rho_0}$, J is the symmetry energy at saturation density ρ_0 and the other parameters like slope (L), curvature (K_{sym}) and skewness (Q_{sym}) are as follow:

$$L = 3\rho \frac{\partial S(\rho)}{\partial \rho} \Big|_{\rho=\rho_0}, \quad (23)$$

$$K_{sym} = 9\rho^2 \frac{\partial^2 S(\rho)}{\partial \rho^2} \Big|_{\rho=\rho_0}, \quad (24)$$

$$Q_{sym} = 27\rho^3 \frac{\partial^3 S(\rho)}{\partial \rho^3} \Big|_{\rho=\rho_0}. \quad (25)$$

In a similar fashion, we can expand the asymmetric NM incompressibility $K(\xi)$ as

$$K(\xi) = K + K_\tau \xi^2 + \mathcal{O}(\xi^4), \quad (26)$$

where K is the incompressibility at the saturation density and

$$K_\tau = K_{sym.} - 6L - \frac{Q_0 L}{K}, \quad (27)$$

TABLE II. The NM properties such as B/A , K , effective mass ratio (M^*/M), symmetry energy (J) and its different co-efficients etc. are listed at the saturation density for five different parameter sets. All the parameters has MeV unit except ρ_0 (fm^{-3}) and M^*/M (dimensionless). The empirical/experimental values are given in the last column with their Refs. [a] [65], [b] [66], [c] [67], [d] [68] and [e] [69–71]

Parameter	NL3	FSUGarnet	G3	IOPB-I	BigApple	Emp./expt.
ρ_0 (fm^{-3})	0.148	0.153	0.148	0.149	0.155	0.148-0.185 [a]
B/A	-16.29	-16.23	-16.02	-16.10	-16.34	-15.00- -17.00 [a]
M^*/M	0.595	0.578	0.699	0.593	0.608	—
J	37.43	30.95	31.84	33.30	31.31	30.20-33.70 [b]
L	118.65	51.04	49.31	63.58	39.80	35.00-70.00 [b]
K_{sym}	101.34	59.36	-106.07	-37.09	90.44	-174- -31 [c]
Q_{sym}	177.90	130.93	915.47	862.70	1114.74	—
K	271.38	229.5	243.96	222.65	227.00	220-260 [d]
Q_0	211.94	15.76	-466.61	-101.37	-195.67	—
K_τ	-703.23	-250.41	-307.65	-389.46	-116.34	-840- -350 [e]
K_{asy}	-610.56	-246.89	-401.97	-418.58	-151.03	—
K_{sat2}	-703.23	-250.41	-307.65	-389.46	-116.34	—

and $Q_0 = 27\rho^3 \frac{\partial^3 \mathcal{E}}{\partial \rho^3}$ in symmetric NM. The NM properties are compared in Table II for various forces used in the present calculations.

III. RESULTS AND DISCUSSIONS

In this section, we discuss the properties of finite nuclei, NM and the NS matter. Some of the finite nuclei properties like binding energy per particle, charge radius, neutron-skin thickness, single-particle energy and two neutron separation energy for few spherical nuclei are analysed. These ground state properties define the nucleus in all respect. The NM parameters such as binding energy per particle, incompressibility, symmetry energy and its different coefficients are studied both for symmetric NM (SNM) and pure neutron matter (PNM). Finally, we extend our calculations to the NS and find its EoS, mass, radius, tidal deformability and the moment of inertia in detail.

A. Finite Nuclei

1. Binding energies, charge radii, and neutron-skin thickness

The binding energy per particle (B/A) is a standard and very precisely measured quantity for a large range of nuclei. Here, we calculate theoretically B/A , charge radii (R_c) and neutron skin thickness (Δr_{np}) for eight spherical nuclei and compared with the experimental results as given in Table III. The BigApple parameter set well satisfies the B/A and R_c of the listed nuclei similar to other parameter sets.

The neutron skin thickness (Δr_{np}) defined as the root mean

TABLE III. The predicted value of B/A and R_c and Δr_{np} are listed with the available experimental data [72, 73].

Nucleus	Obs.	Expt.	NL3	FSUGarnet	G3	IOPB-I	BigApple
^{16}O	B/A	7.976	7.917	7.876	8.037	7.977	7.882
	R_c	2.699	2.714	2.690	2.707	2.705	2.713
	Δr_{np}		-0.026	-0.028	-0.028	-0.027	-0.027
^{40}Ca	B/A	8.551	8.540	8.528	8.561	8.577	8.563
	R_c	3.478	3.466	3.438	3.459	3.458	3.447
	Δr_{np}		-0.046	-0.051	-0.049	-0.049	-0.049
^{48}Ca	B/A	8.666	8.636	8.609	8.671	8.638	8.547
	R_c	3.477	3.443	3.426	3.466	3.446	3.447
	Δr_{np}		0.229	0.169	0.174	0.202	0.170
^{68}Ni	B/A	8.682	8.698	8.692	8.690	8.707	8.669
	R_c		3.870	3.861	3.892	3.873	3.877
	Δr_{np}		0.262	0.184	0.190	0.223	0.171
^{90}Zr	B/A	8.709	8.695	8.693	8.699	8.691	8.691
	R_c	4.269	4.253	4.231	4.276	4.253	4.239
	Δr_{np}		0.115	0.065	0.068	0.091	0.069
^{100}Sn	B/A	8.258	8.301	8.298	8.266	8.284	8.259
	R_c		4.469	4.426	4.497	4.464	4.445
	Δr_{np}		-0.073	-0.078	-0.079	-0.077	0.076
^{132}Sn	B/A	8.355	8.371	8.372	8.359	8.352	8.320
	R_c	4.709	4.697	4.687	4.732	4.706	4.695
	Δr_{np}		0.349	0.224	0.243	0.287	0.213
^{208}Pb	B/A	7.867	7.885	7.902	7.863	7.870	7.894
	R_c	5.501	5.509	5.496	5.541	5.52	5.495
	Δr_{np}		0.283	0.162	0.180	0.221	0.151

square radii difference of neutron and proton distribution, i.e. $\Delta r_{np} = R_n - R_p$. Electron scattering experiments can easily determine the charge distribution of protons in the nucleus. Still, it isn't straightforward to determine the neutron distributions in nuclei in a model-independent way. The Lead Radius Experiment (PREX) at JLAB has been designed to measure the radius of the neutron distribution in ^{208}Pb from parity violation by the weak interaction. From this measurement, it is determined large uncertainties in the measurement of the neutron radius of ^{208}Pb [74]. Hopefully, the PREX-II experiment will provide more insight not only on neutron skin-thickness with great precision but also to the understanding of the EoS for NM and thus improve our understanding of NSs. On the other hand, the neutron-skin thickness of 26 stable nuclei starting from ^{40}Ca to ^{238}U has deduced by using anti-protons experiment from the low Energy anti-proton ring at CERN [75]. The numerically calculated results and experimental data with an error bar is shown in Fig. 1.

$$\Delta r_{np} = (0.90 \pm 0.15)I + (-0.03 \pm 0.02) \text{ fm}. \quad (28)$$

The fitted values for Δr_{np} are placed as band in Fig. 1. The calculated skin-thickness of the 26 nuclei for BigApple parameter set are matching well as good as other sets. The skin-thickness for ^{208}Pb nuclei with BigApple is 0.151 fm, which lies in the range given by the proton elastic scattering experi-

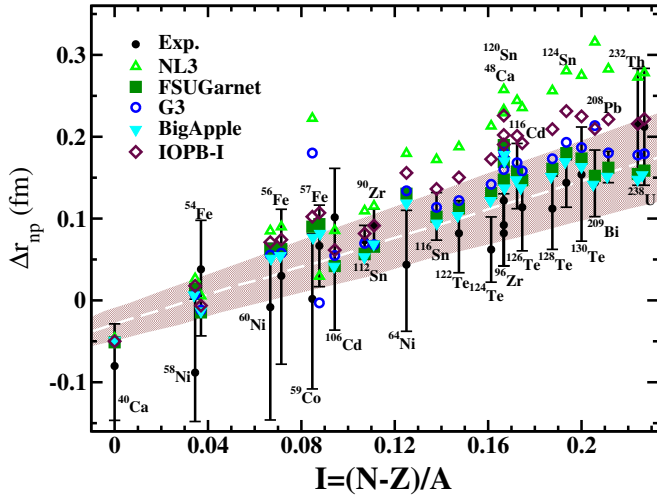


FIG. 1. (color online) The neutron-skin thickness as a function of the asymmetry parameter. Results obtained with five different parameter sets are compared with experimental data [75]. The shaded region is depicted using the fitting formula in Eq. (28).

ment [76], $\Delta r_{np} = 0.148\text{--}0.265$ fm.

2. Single-particle energy

The study of single-particle energies for nuclei gives us the indication of shell spacing. From this, we can identify large shell gaps and predict the presence of magic numbers. Here, we calculate the single particle energies of two doubly magic nuclei as representative cases, for e.g. ^{48}Ca and ^{208}Pb with IOPB-I, BigApple and NL3 parameter sets. The predicted single-particle energies for both protons and neutrons of ^{48}Ca and ^{208}Pb are compared with the experimental data [77] in Figs. 2 and 3. The prediction of BigApple parameter set almost satisfy the experimental data as compare to the other parameter sets. The known magic numbers 20, 28, 82 and 126 are reproduced by all three parameter sets. The nuclei, ^{48}Ca and ^{208}Pb are doubly closed, which are considered to be perfectly spherical. The energy levels are degenerate states, i.e. same energy for all the nucleons in a particular orbitals as clearly visible in the figure.

3. Two-neutron separation energy $S_{2n}(Z, N)$

The two neutron separation energy $S_{2n}(N, Z)$ is the energy required to remove two neutrons from a nucleus with N neutrons and Z protons, i.e.

$$S_{2n}(N, Z) = B(N, Z) - B(N - 2, Z). \quad (29)$$

The study of neutron separation energies is essential to explore the nuclear structure near the drip line. A sudden drop in $S_{2n}(N, Z)$ represents the beginning of a new shell. The large shell gap in single-particle energy levels indicates the magic number, and it is responsible for the extra stability for

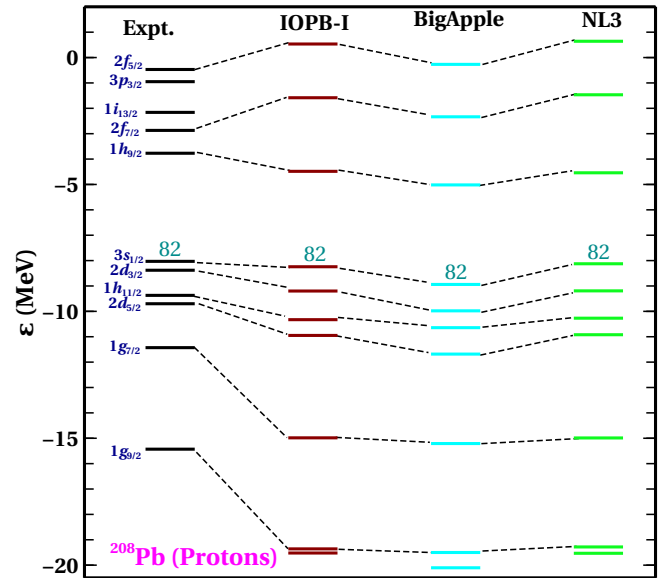
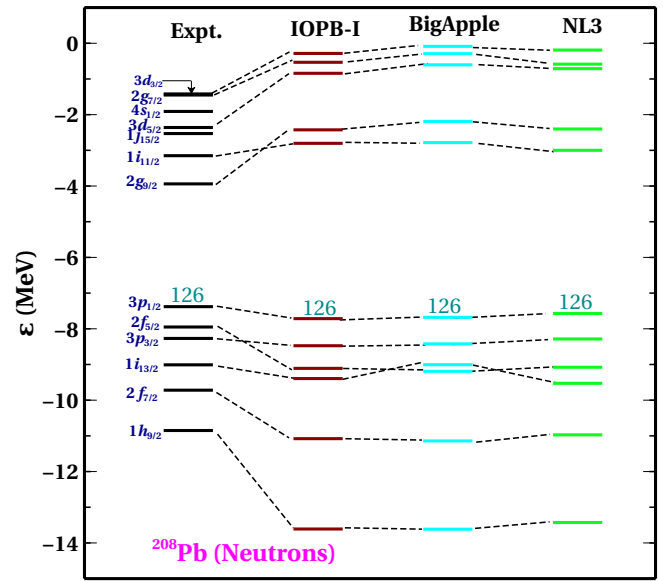


FIG. 2. (colour online) The single-particle energies of ^{208}Pb for IOPB-I, BigApple and NL3 are compared with experimental data [77]. The last occupied level is also shown with the numbers 126 for neutrons and 82 for protons.

the magic nuclei. We calculate the S_{2n} for six isotopic chains Ca, Ni, Zr, Sn, Pb and $Z=120$, which are shown in Fig. 4 and compare with experimental data given in the Ref. [72]. We also compare the results obtained for the $Z=120$ isotopic chain with finite range droplet model (FRDM) [78]. From Fig. 4, it is cleared that the value of S_{2n} decreases with the increase of the neutron number, i.e. towards the neutron drip line. All the magic characters appear at different neutron number $N=20, 28, 32, 40, 50, 82, 126$. The predictions of BigAp-

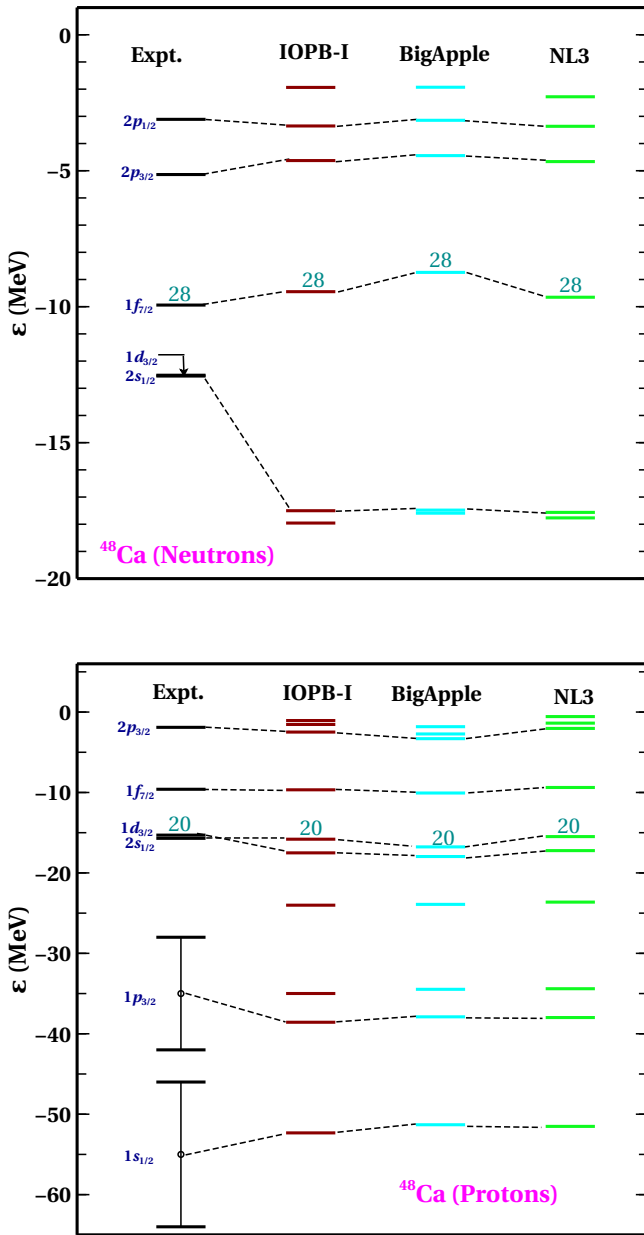


FIG. 3. (colour online) Same as Fig. 2, but for ^{48}Ca .

ple are also reasonably satisfied like other parameter sets. In the last part of Fig. 4, the magicity arises at $N=172, 184, 198$ for $Z=120$ nuclei. In this case, we compare the calculated data with FRDM [78], since it has no experimental data for $Z=120$. The sharp falls in the S_{2n} for five different parameter sets, which are consistent with the prediction of various models in the superheavy mass region [79–82]. Bhuyan and Patra [83] predicted that $Z=120$ is the magic number after $Z=82$, which lies in the superheavy region. Also, in the Ref. [82], they have predicted that $Z=120$ nuclei are spherical in their ground state. We hope the future experiments may have answer to the shell

closure at $Z=172, 184$ and 198 .

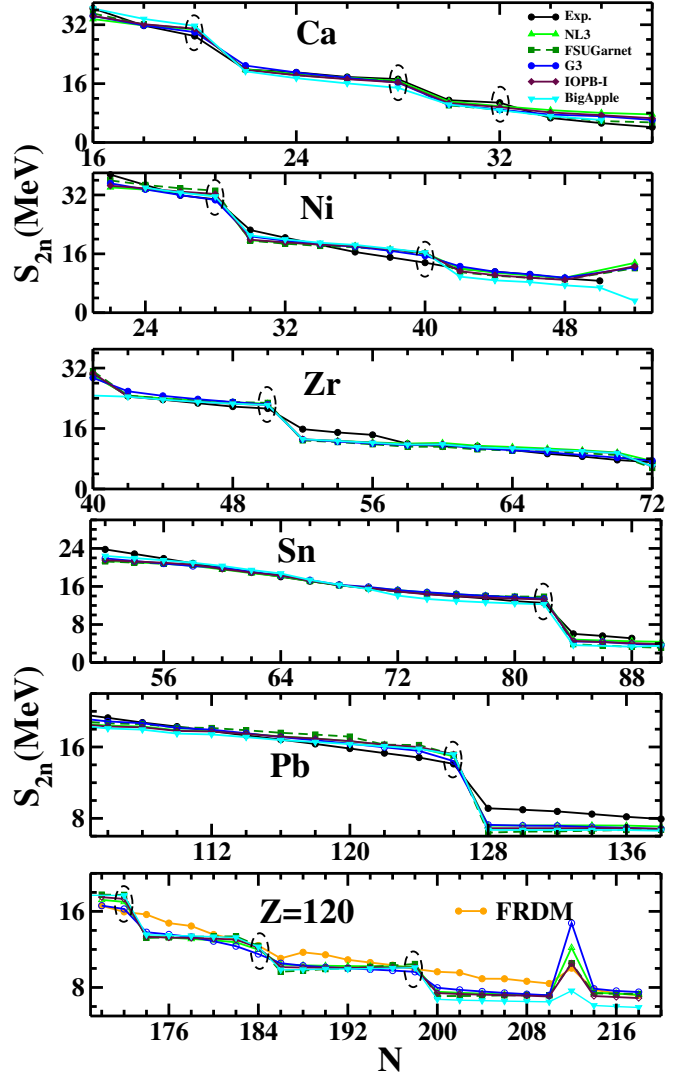


FIG. 4. (colour online) The two-neutron separation energy as a function of neutron number for the isotopic nuclei like Ca, Ni, Zr, Sn and Pb for five different parameter sets. The FRDM [78] data and experimental data [72] are also given for comparison. The circle represents the magicity of the nuclei.

B. Nuclear Matter

In this sub-section, we study NM parameters like BE per nucleons B/N , incompressibility K , density-dependent symmetry energy $S(\rho)$ and its different coefficients like slope L , curvature K_{sym} , skewness Q_{sym} etc. in detail. Here we give special emphasis on the newly developed parameter set BigApple [27]. The values of NM quantities are given in Table II. First, we discussed the incompressibility of the NM. For BigApple, the value of $K=227.0$ MeV, which lies in the experimental data range determined from the iso-scalar giant monopole resonance (ISGMR) [68, 69] and its value is

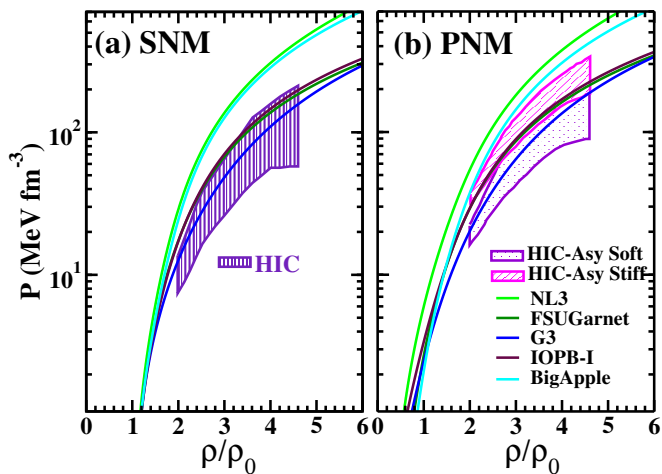


FIG. 5. (colour online) Calculated pressure with the variation of baryon density. The results for NL3, BigApple, FSUGarnet, G3 and IOPB-I are compared with HIC data [60] both for symmetric nuclear matter (left) and pure neutron matter (right). For PNM case, the same data is divided to (i) HIC-Asy soft (ii) HIC-Asy stiff, which is mainly divided on the basis of the density dependence symmetry energy.

$K = 240 \pm 20$ MeV obtained from ^{90}Zr and ^{208}Pb data. The values of symmetry energy and its slope for BigApple are 33.31 and 39.80 MeV, which are also in the range given by Danielewicz and Lee [66] at the saturation density (see Table II). Recently the value of K_{sym} is constrained by Zimmerman *et al.* [67] combining the GW170817 and NICER data and it is found to be 102^{+71}_{-72} MeV at 1σ level. Except for IOPB-I and G3, none of the parameter sets able to reproduce the data including NL3 and BigApple. The other parameters K_τ for BigApple parameter also don't lie in the range given in Table II.

First, we display in Fig. 5, the pressure with the variation of the baryon density both for SNM and PNM. Then we compare with the experimental flow data [60]. The determined pressure of the parameter sets like G3 show excellent agreement with heavy-ion collisions (HIC) data for the whole densities range for SNM (shown in Fig. 5). Although the parameter sets IOPB-I and FSUGarnet give stiffer EoS as compared to G3, still matches with HIC data. NL3 and BigApple are the stiffest EoSs as compared to others. So they disagree with the HIC data both for SNM and PNM cases. Though the EoS for BigApple parameter doesn't pass through the experimental shaded regions given by HIC, still it predicts the value of K , J and L which reasonably match with the empirical/experimental values as given in Table II.

Next, our focus is on the binding energy per nucleon (B/N), which is a precisely measured quantity at the saturation density. The variation of B/N with neutron density (ρ_n/ρ_0) for PNM system, is shown in Fig. 6 for BigApple parameter set along with NL3, FSUGarnet, G3 and IOPB-I. Some experimental data are also put for comparison in Fig. 6. From this plot, one can see that at the low-density regions (in inset plot), except BigApple and NL3, others parameter sets are in harmony with the results obtained from the microscopic

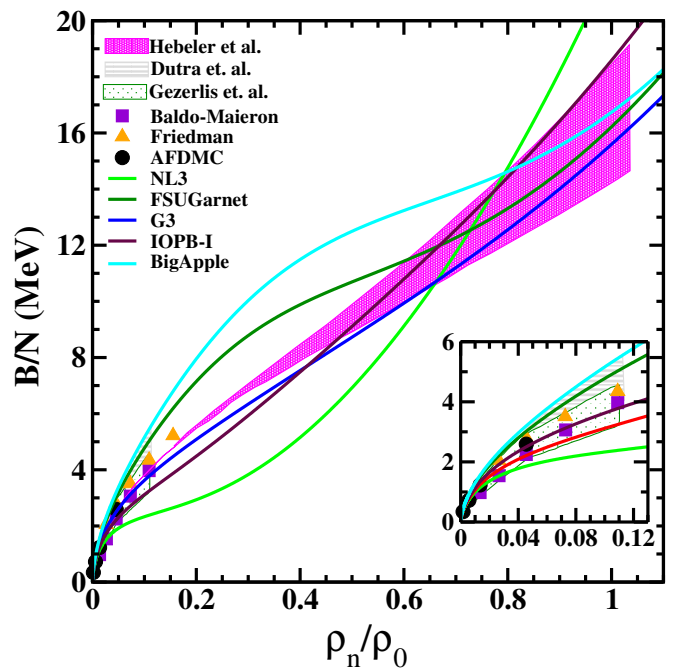


FIG. 6. (color online) The B/N as a function of neutron density with NL3 [4], FSUGarnet [45], G3 [8], IOPB-I [9] and BigApple [27] parameter sets. The other results are from Hebel *et al.* [84], Dutra *et al.* [13], Gezerlis *et al.* [85], Baldo-Maieron [86], Friedman [87] and Auxiliary-field diffusion Monte Carlo (AFDMC) [88].

calculations. At high densities, the BigApple, G3, IOPB-I and FSUGarnet are perfectly passed through the shaded regions. It means that these parameters sets are consistent with results obtained by the Hebel *et al.* [84] at the high-density limit. It indicates that these parameter sets have been taken the two-nucleon ($2N$) and three-nucleon ($3N$) interactions in their calculations. The B/A of all models lies in the empirical limit, which is given in Table II.

The symmetry energy is defined as the energy difference between PNM and SNM. Although the symmetry energy is known at the saturation to some extent but the density dependence symmetry energy is very fuzzy. It has a broad relation on the NS properties. There are some recent references [26, 92–94], which are basically related symmetry energy with NS properties. It has diverse behaviour at the different densities regions [61]. In Fig. 7, we have shown the density-dependent symmetry energy with baryon density for five different parameter sets. The symmetry energy for G3, IOPB-I and FSUGarnet have softer symmetry energy at the low density due to the presence of cross-coupling between ω and ρ meson which is consistent with HIC Sn+Sn [89, 90] and IAS [66] data as shown in Fig. 7. On the other hand, BigApple predicts the softer $S(\rho)$ at a higher density, which doesn't pass through the ASY data [91].

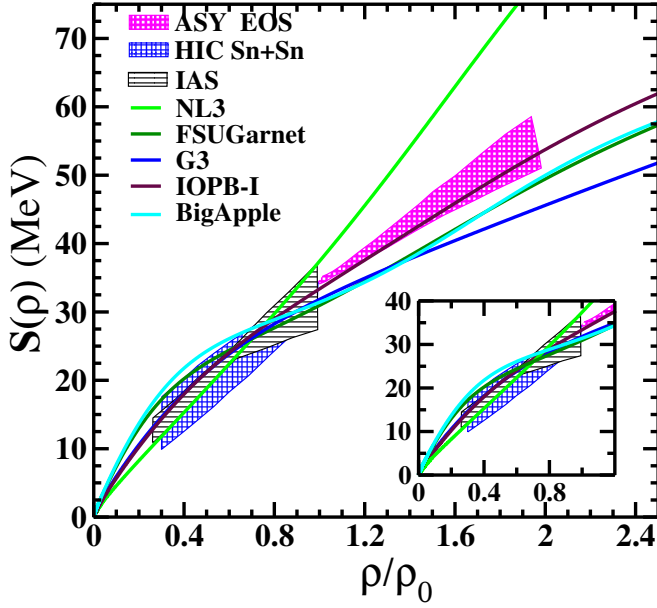


FIG. 7. (color online) The density dependent symmetry energy with the baryon density for five different parameter sets. The shaded region is the symmetry energy from IAS [66], HIC Sn+Sn [89, 90] and ASY-EoS experimental data [91]. The zoomed pattern of the symmetry energy at low densities is shown in the inset.

C. Neutron Star

1. Equation of state of the NS

To study NS properties, the EoS is the main ingredient while solving the star equations. We calculate the core EoS in Eqs. (17) and (18) with the addition of both β -equilibrium and charge neutrality conditions [95]. For the crust part, we take the BCPM EoS [96] (both for inner and outer). We add core with crust EoS to form an unified EoS which is shown in Fig. 8. The shaded regions are for 50% (grey) and 90% (yellow) credible limit given by GW170817 data [2]. The EoS for BigApple almost passes through the shaded region similar to G3, IOPB-I and FSUGarnet. The EoS for BigApple passes through the GW data of the NS and also predict the maximum mass and canonical radius as $2.60 M_{\odot}$ and 12.96 km respectively, which are well satisfied with GW190814 data [3].

2. Mass, Radius, Tidal deformability and moment of inertia

Here, we calculate the mass, radius and tidal deformability of a non-rotating neutron star. When the NS is in the presence of static external tidal field \mathcal{E}_{ij} that results the deformation in the star. Such deformation is quantified as the tidal deformability, which is defined as [97, 98]

$$\lambda = -\frac{Q_{ij}}{\mathcal{E}_{ij}} = \frac{2}{3}k_2R^5, \quad (30)$$

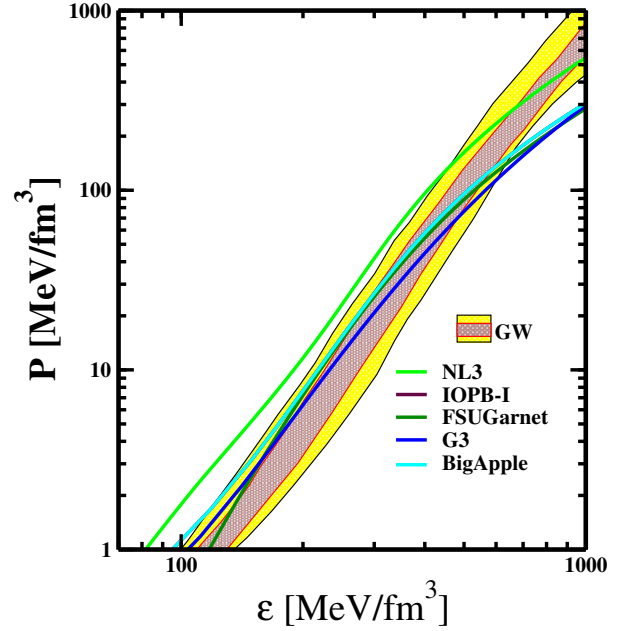


FIG. 8. (color online) The equations of states of β -equilibrated matter for NL3, FSUGarnet, G3, IOPB-I and BigApple parameter sets. The shaded regions are for 50 % (orange) and 90% (grey) posterior credible limit given by the GW170817 data [2].

and

$$\Lambda = \frac{\lambda}{M^5} = \frac{2k_2}{3C^5}, \quad (31)$$

where Q_{ij} is the induced quadrupole moment of a star in binary, and \mathcal{E}_{ij} is the static external quadrupole tidal field of the companion star. λ is the tidal deformability and k_2 is the second love number [97, 99]. Λ is the dimensionless tidal deformability, and C is the compactness parameter ($C = M/R$). Both R and k_2 are fixed for a stellar mass which is predicted by the EoS of the NS and the value of k_2 is 0.05–0.15 for a realistic star [100]. The love number expression is given as [97]

$$k_2 = \frac{8}{5}(1 - 2C)^2C^5[2C(y - 1) - y + 2] \left\{ 2C(4(y + 1)C^4 + (6y - 4)C^3 + (26 - 22y)C^2 + 3(5y - 8)C - 3y + 6) - 3(1 - 2C)^2(2C(y - 1) - y + 2) \log\left(\frac{1}{1 - 2C}\right) \right\}^{-1}. \quad (32)$$

The value of $y \equiv y(R)$ can be computed by solving the differential equation as [98, 100]

$$r \frac{dy(r)}{dr} + y(r)^2 + y(r)F(r) + r^2Q(r) = 0, \quad (33)$$

where

$$F(r) = \frac{r - 4\pi r^3[\mathcal{E}(r) - P(r)]}{r - 2M(r)}, \quad (34)$$

$$Q(r) = \frac{4\pi r(5\mathcal{E}(r) + 9P(r) + \frac{\mathcal{E}(r)+P(r)}{\partial P(r)/\partial \mathcal{E}(r)} - \frac{6}{4\pi r^2})}{r - 2M(r)} - 4 \left[\frac{M(r) + 4\pi r^3 P(r)}{r^2(1 - 2M(r)/r)} \right]^2. \quad (35)$$

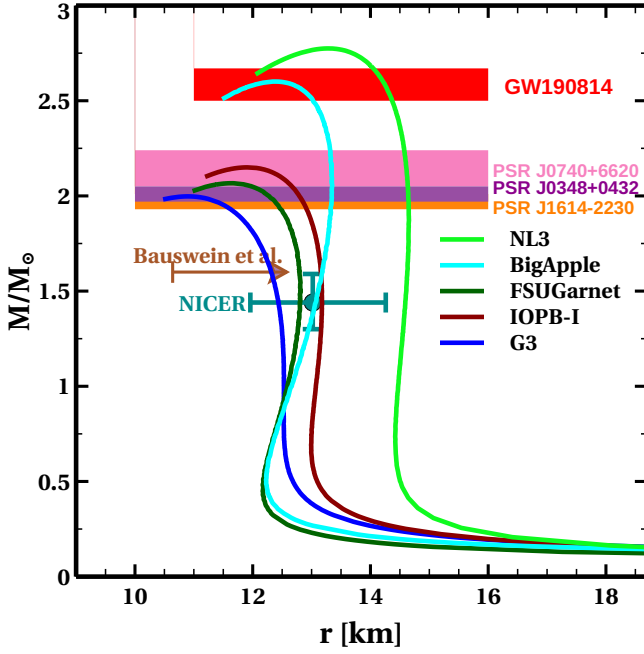


FIG. 9. (color online) The mass-radius profile predicted by NL3, FSUGarnet, G3, IOPB-I and BigApple. The different colour bands shows the mass of the NS observed from the different pulsars. The mass constraint by GW190814 [3] and NICER [40] results are also depicted.

The estimation of the λ of a star can be done by integrating Eq. (33) simultaneously with Tolman-Oppenheimer-Volkov (TOV) equations [101, 102] for a given EoS.

$$\frac{dP(r)}{dr} = -\frac{[\mathcal{E}(r) + P(r)][M(r) + 4\pi r^3 P(r)]}{r^2(1 - \frac{2M(r)}{r})}, \quad (36)$$

and

$$\frac{dM(r)}{dr} = 4\pi r^2 \mathcal{E}(r). \quad (37)$$

The boundary conditions are $P(0) = P_c$, $M(0)=0$, and $y(0) = 2$. To calculate the love number, we solve these Eqs. (30-37) for a given EoS of the star at $r=0$. At the surface of the star $P(R) = 0$, $M(R) = M$ and $r(R) = R$. Thus, for each central density we have uniquely determined the mass M , the radius R and the love number k_2 for an isolated NS.

The mass and radius of the NS for five different parameter sets are shown in Fig. 9. The horizontal bars are the precise measured NS masses from PSR J1614-2230 [54], PSR J0348+0432 [103], PSR J0740+6620 [28] and recently measured from the NS-black hole coalescence event GW190814 [3]. The canonical radius constraint given by the NICER [40, 41] is also shown.

The calculated maximum mass and radius for the BigApple parameter set are found to be $2.60 M_\odot$ and 12.41 km. These values for the other four assumed parameter sets are given in Table IV. The maximum mass and canonical radius of the BigApple satisfies the GW190814 limit (2.50 - $2.67 M_\odot$) and NICER data (11.96 - 14.26 km) respectively. Recently, the

maximum mass limit is $2.01 \pm 0.04 \lesssim M/M_\odot \lesssim 2.16 \pm 0.03$, which has been constrained by Rezzolla et al. [104] combining the GW observations of the merger of two NSs and quasi-universal relations. The lower limit ranges come from the pulsar observational data. The maximum mass for G3, FSUGarnet and IOPB-I lie within the limit given by Rezzolla et al. except for NL3 and BigApple. The canonical radius for different sets well passes through the green band predicted by the NICER data [41, 105] except for NL3. Also the $R_{1.4}$ and $\Lambda_{1.4}$ for BigApple well aligned with constrained from GW190814 [3] ($12.9^{+0.8}_{-0.7}$ km and 616^{+273}_{-158}).

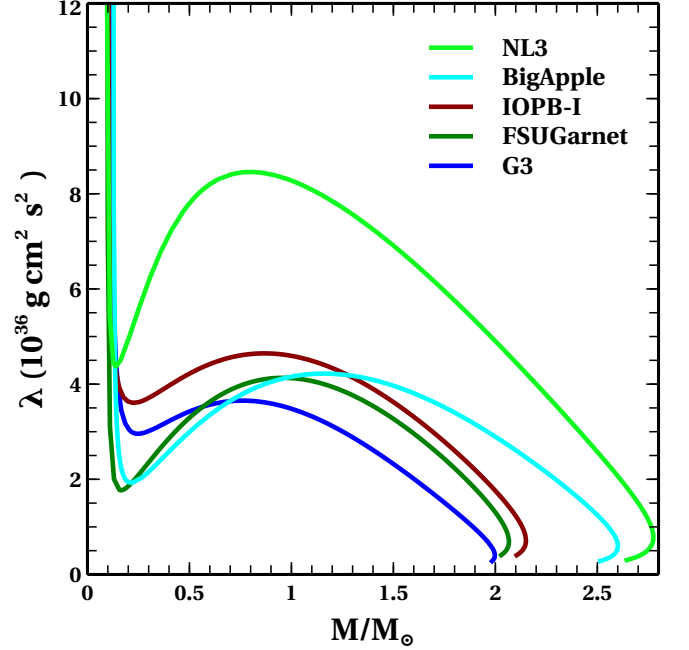


FIG. 10. (colour online) The tidal deformability λ as a function of NS mass with different parameter sets.

The tidal deformability of the NS mainly depends on the structure of the NS and radius, which developed due to the tidal quadrupole by its companion. The calculated values of λ (from Eq. 30) for 2nd order perturbation ($l = 2$) as depicted in Fig. 10 for BigApple along with other four different parameter sets. From Eq. 30, λ directly depends on the k_2 and R^5 , which means as the radius of the NS increases the value of λ goes on increasing and maximum at the surface. It is a general notion that λ is more for stiffer EoS than the softer one. For NL3, the predicted value of λ is more than other sets (IOPB-I, G3) due to its stiffer EoS. On the other hand, BigApple has a similar stiff EoS as of NL3. Contrary to the common understanding, it predicts a comparable λ with that of IOPB-I and G3 sets. This is because the BigApple predicts similar NS radius as these two sets. It is thus, worthwhile to note that the nature of EoS doesn't decide the value of λ much, but the radius of the NS plays an important role for the tidal deformation of the surface.

In Fig. 11, we depicted the dimensionless tidal deformability Λ for the binary NS for the five parameter sets. The individual dimensionless tidal deformabilities Λ_1 and Λ_2 cor-

TABLE IV. The maximum mass (M_{max}), central density (\mathcal{E}_c), radius (R), dimensional tidal deformability (Λ), compactness (C) and dimensionless canonical moment of inertia ($\bar{I}_{1.4}$) are given both for canonical (1.4) and massive NS for BigApple along with other four different parameter sets.

Model	$M_{max.}$ (M_\odot)	\mathcal{E}_c	R	Λ		C		$\bar{I}_{1.4}$
		(MeV/fm^3)	(km)	1.4	max.	1.4	max.	
NL3	2.77	270 870	14.58 13.28	1267.79	4.49	0.096	0.209	16.970
BigApple	2.60	326 980	12.96 12.41	717.30	5.00	0.108	0.209	14.538
IOPB-I	2.15	366 1100	13.17 11.91	681.27	14.82	0.106	0.180	14.278
FSUGarnet	2.07	384 1120	12.87 11.71	624.81	18.20	0.109	0.176	13.940
G3	1.99	460 1340	12.46 10.93	461.28	12.16	0.112	0.183	12.857

respond to the higher and lower mass m_1 and m_2 respectively [1]. The chirp mass is defined as

$$\mathcal{M}_c = \frac{(m_1 m_2)^{3/5}}{(m_1 + m_2)^{1/5}}, \quad (38)$$

where m_1 and m_2 are the masses of the two binary star. The chirp mass is quite accurately measured quantity and its value is $1.188^{+0.0004}_{-0.0002} M_\odot$ [1]. Here, we calculate the m_1 by varying the m_2 in the range $1.17 < m_2/M_\odot < 1.36$ fixing the chirp mass $\mathcal{M}_c = 1.188 M_\odot$ for low-spin scenario [1]. The predicted values of Λ_1 and Λ_2 for BigApple sit within the 50% and 90% contour from the GW170817 [1]. From Fig. 11, it is concluded that the softer EoS gives less Λ as compared to stiffer one. The values of $\Lambda_{1.4}$ is predicted by the BigApple parameter as 717.30, which is not aligned within the limit given by the GW170817 of $\Lambda_{1.4} = 190^{+390}_{-120}$ at the 90% confidence level [2]. This limit can be achieved by the softer EoS only. The values of Λ for different parameter sets are given in Table IV.

The moment of inertia (MI) of a slowly rotating NS (for a spherical star) is given by

$$I \approx \frac{8\pi}{3} \int_0^R (\mathcal{E} + P) e^{-\phi(r)} \left[1 - \frac{2m(r)}{r} \right]^{-1} \frac{\bar{\omega}}{\Omega} r^4 dr, \quad (39)$$

where $\bar{\omega}$ and Ω are the dragging rotational functions and angular velocity respectively for the uniformly rotating NS [106, 107]. The Eq. (39) is solved together with TOV Eqs. (36) and (37) for a spherically symmetric NS. From Eq. (39), the MI depends on both the EoS of the NS and mass enclosed at some radius. Naively we say that it depends on the structure of the body. In Fig. 12, we present the dimensionless MI with the mass of the NS. The MI decreases with the increase of mass of the star. From this Table IV, it is clear that the stiffer EoS like NL3 gives higher canonical MI than the softer one. The measurement of MI for the NS which is believed to be Universal, i.e. which is independent of the EoS [108, 109] and it can constraint the EoS at the supra-saturation density.

IV. SUMMARY AND CONCLUSIONS

Recently the LVC detected the collision of a black-hole of mass $22.2\text{-}24.3 M_\odot$ with a compact object of mass $2.50\text{-}2.67$

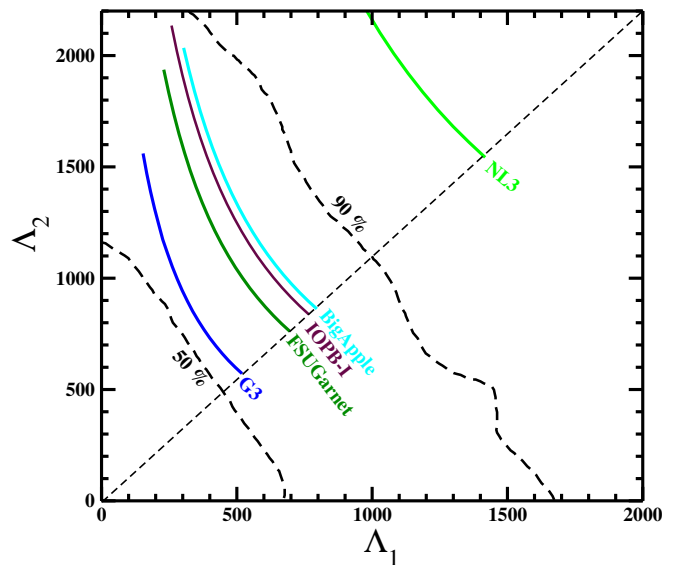


FIG. 11. (color online) Binary NS tidal deformabilities calculated for NL3, FSUGarnet, G3, IOPB-I and BigApple sets are compared with the 50% and 90% probability contour in case of low-spin scenario $|\chi| \leq 0.05$ as given by GW170817 [1].

M_\odot which is named as GW190814 event. The secondary component of the GW190814 event is either a super-massive NS or light black-hole because it has no tidal signatures and electromagnetic counterparts in the waveform. Fattoyev *et al.* constructed an EDF parameter set known as BigApple, which predicts the mass of the compact object $2.60 M_\odot$. The predictive power of BigApple for finite nuclei is as good as other RMF/E-RMF forces which are designed for finite nuclei calculations. These sets are also reproduced the NM and NS properties to a satisfactory extent. Contrary to IOPB-I and G3 sets, the BigApple fails to reproduce the flow data given by Danielewicz *et al.* [66].

In this present paper, we systematically studied the nuclear bulk properties such as binding energy per particle, charge radius, neutron-skin thickness, two-neutron separation energy and single-particle energy etc. for the magic nuclei Ca, Ni, Zr, Sn, Pb and $Z=120$ in the whole isotopic chains. The results of BigApple are compared with the NL3, IOPB-I, G3 and FSUGarnet sets. It is found that all the finite nuclei

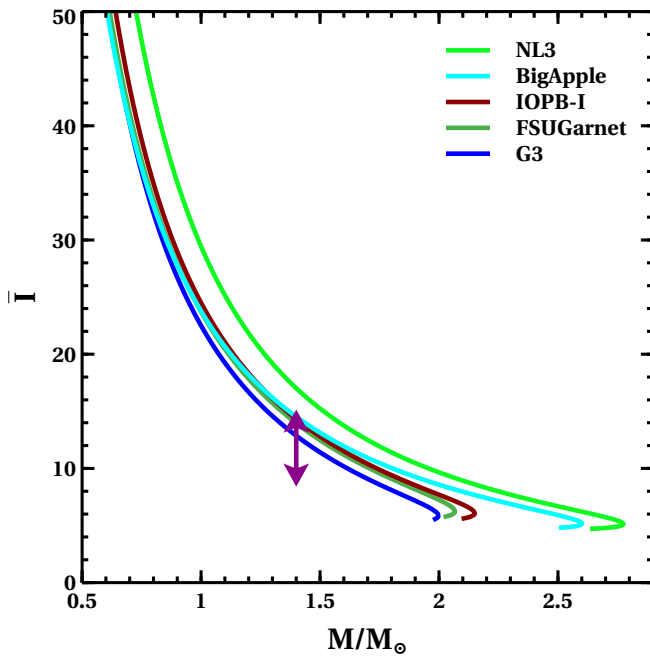


FIG. 12. (colour online) The dimensionless moment of inertia with the mass of the NS for different parameter sets. The overlaid arrows represent the MI constraint from the analysis of PSR J0737-3039A [108, 109].

properties predicted by BigApple are well satisfied with the experimental data for the series of nuclei. The NM properties such as incompressibility, symmetry energy and its slope are also consistent with empirical/experimental data available till now. The BigApple predicted the maximum mass and canonical radius of the NS as $2.60 M_{\odot}$ and 12.96 km, respectively, which are consistent with GW190814 data. The canonical radius is also satisfied with NICER data. The calculated $\Lambda_{1.4}$ of the BigApple is 717.30, which is well suited with GW190814 data, but it fails to reproduce the GW170817 data due to its stiff EoS. Since the predicted EoS of the NM doesn't consistent with flow data, refitting of the parameter is in demand. It is important to note that every coupling has its own importance. For example, the self-coupling of the σ -mesons reduces the incompressibility considerably. Similarly, the self-coupling of the ω -meson softens the EoS. The cross-coupling of the ω - and ρ -mesons controls the neutron radius of finite nuclei, which has also a significant role in the radius of the NS. Based on these natures of the couplings, one can match the EoS with the flow data keeping the mass of the NS which consistent with GW190814 data. We hope one can do the fine-tuning of the parameters along with additional couplings which can satisfy the current issue as well as the flow data.

Acknowledgments: SKB is supported by the National Natural Science Foundation of China Grant No. 11873040.

-
- [1] B. P. Abbott, R. Abbott, T. D. Abbott, *et al.* (The LIGO Scientific Collaboration and Virgo Collaboration), *Phys. Rev. Lett.* **119**, 161101 (2017), arXiv:1710.05832 [gr-qc].
- [2] B. P. Abbott, R. Abbott, T. D. Abbott, *et al.* (The LIGO Scientific Collaboration and the Virgo Collaboration), *Phys. Rev. Lett.* **121**, 161101 (2018), arXiv:1805.11581 [gr-qc].
- [3] R. Abbott, T. D. Abbott, S. Abraham, *et al.*, *The Astrophysical Journal* **896**, L44 (2020), arXiv:2006.12611 [astro-ph.HE].
- [4] G. A. Lalazissis, J. König, and P. Ring, *Phys. Rev. C* **55**, 540 (1997), arXiv:9607039 [nucl-th].
- [5] R. J. Furnstahl, B. D. Serot, and H.-B. Tang, *Nucl. Phys. A* **615**, 441 (1997), arXiv:9608035 [nucl-th].
- [6] P. G. Reinhard, *Z. Phys. A Atomic Nuclei* **329**, 257 (1988).
- [7] S. K. Singh, M. Bhuyan, P. K. Panda, and S. K. Patra, *Journal of Physics G: Nuclear and Particle Physics* **40**, 085104 (2013), arXiv:1211.5461 [nucl-th].
- [8] B. Kumar, S. Singh, B. Agrawal, and S. Patra, *Nuclear Physics A* **966**, 197 (2017), arXiv:1705.02621 [nucl-th].
- [9] B. Kumar, S. K. Patra, and B. K. Agrawal, *Phys. Rev. C* **97**, 045806 (2018), arXiv:1711.04940 [nucl-th].
- [10] E. Chabanat, P. Bonche, P. Haensel, J. Meyer, and R. Schaeffer, *Nucl. Phys. A* **635**, 231 (1998).
- [11] B. Alex Brown, *Phys. Rev. C* **58**, 220 (1998).
- [12] J. Stone and P.-G. Reinhard, *Progress in Particle and Nuclear Physics* **58**, 587657 (2007), arXiv:nucl-th/0607002 [nucl-th].
- [13] M. Dutra, O. Lourenço, J. S. Sá Martins, *et al.*, *Phys. Rev. C* **85**, 035201 (2012), arXiv:1202.3902 [nucl-th].
- [14] T. Nikšić, D. Vretenar, P. Finelli, and P. Ring, *Phys. Rev. C* **66**, 024306 (2002).
- [15] S. Typel, *Phys. Rev. C* **71**, 064301 (2005).
- [16] G. A. Lalazissis, T. Nikšić, D. Vretenar, and P. Ring, *Phys. Rev. C* **71**, 024312 (2005).
- [17] T. Klähn, D. Blaschke, S. Typel, *et al.*, *Phys. Rev. C* **74**, 035802 (2006), arXiv:nucl-th/0602038 [nucl-th].
- [18] E. R. Most, L. J. Papenfort, L. R. Weih, and L. Rezzolla, (2020), arXiv:2006.14601 [astro-ph.HE].
- [19] K. Vattis, I. S. Goldstein, and S. M. Koushiappas, (2020), arXiv:2006.15675 [astro-ph.HE].
- [20] I. Tews, P. T. H. Pang, T. Dietrich, *et al.*, (2020), arXiv:2007.06057 [astro-ph.HE].
- [21] Y. Lim, A. Bhattacharya, J. W. Holt, and D. Pati, (2020), arXiv:2007.06526 [nucl-th].
- [22] Z. Roupas, (2020), arXiv:2007.10679 [gr-qc].
- [23] D. A. Godzieba, D. Radice, and S. Bernuzzi, (2020), arXiv:2007.10999 [astro-ph.HE].
- [24] K. Huang, J. Hu, Y. Zhang, and H. Shen, (2020), arXiv:2008.04491 [nucl-th].
- [25] H. Tan, J. Noronha-Hostler, and N. Yunes, (2020), arXiv:2006.16296 [astro-ph.HE].
- [26] Y. Zhang, M. Liu, C.-J. Xia, Z. Li, and S. K. Biswal, *Phys. Rev. C* **101**, 034303 (2020), arXiv:2002.10884 [nucl-th].
- [27] F. J. Fattoyev, C. J. Horowitz, J. Piekarewicz, and B. Reed, (2020), arXiv:2007.03799 [nucl-th].
- [28] H. T. Cromartie, E. Fonseca, S. M. Ransom, P. B. Demorest, *et al.*, *Nature Astronomy* **4**, 7276 (2019), arXiv:1904.06759 [astro-ph.HE].
- [29] B. Margalit and B. D. Metzger, *The Astrophysical Journal* **850**, L19 (2017), arXiv:1710.05938 [astro-ph.HE].

- [30] M. Dutra, O. Lourenço, S. S. Avancini, *et al.*, *Phys. Rev. C* **90**, 055203 (2014), arXiv:1405.3633 [nucl-th].
- [31] A. Bauswein, O. Just, H.-T. Janka, and N. Stergioulas, *The Astrophysical Journal* **850**, L34 (2017).
- [32] E. Annala, T. Gorda, A. Kurkela, and A. Vuorinen, *Phys. Rev. Lett.* **120**, 172703 (2018), arXiv:1711.02644 [astro-ph.HE].
- [33] F. J. Fattoyev, J. Piekarewicz, and C. J. Horowitz, *Phys. Rev. Lett.* **120**, 172702 (2018), arXiv:1711.06615 [nucl-th].
- [34] D. Radice, A. Perego, F. Zappa, and S. Bernuzzi, *The Astrophysical Journal* **852**, L29 (2018), arXiv:1711.03647 [astro-ph.HE].
- [35] T. Malik, N. Alam, M. Fortin, and Fofthers, *Phys. Rev. C* **98**, 035804 (2018).
- [36] E. R. Most, L. R. Weih, L. Rezzolla, and J. Schaffner-Bielich, *Phys. Rev. Lett.* **120**, 261103 (2018), arXiv:1803.00549 [gr-qc].
- [37] I. Tews, J. Margueron, and S. Reddy, *Phys. Rev. C* **98**, 045804 (2018), arXiv:1804.02783 [nucl-th].
- [38] R. Nandi, P. Char, and S. Pal, *Phys. Rev. C* **99**, 052802 (2019), arXiv:1809.07108 [astro-ph.HE].
- [39] C. D. Capano, I. Tews, S. M. Brown, *et al.*, *Nature Astronomy* **4**, 625632 (2020), arXiv:1908.10352 [astro-ph.HE].
- [40] M. C. Miller, F. K. Lamb, A. J. Dittmann, *et al.*, *APJ* **887**, L24 (2019), arXiv:1912.05705 [astro-ph.HE].
- [41] T. E. Riley, A. L. Watts, S. Bogdanov, *et al.*, *APJ* **887**, L21 (2019), arXiv:1912.05702 [astro-ph.HE].
- [42] S. Bogdanov, F. K. Lamb, S. Mahmoodifar, *et al.*, *APJ* **887**, L26 (2019), arXiv:1912.05707 [astro-ph.HE].
- [43] G. Raaijmakers, T. E. Riley, A. L. Watts, *et al.*, *Astrophys. J* **887**, L22 (2019), arXiv:1912.05703 [astro-ph.HE].
- [44] S. K. Singh, S. K. Biswal, M. Bhuyan, and S. K. Patra, *Journal of Physics G: Nuclear and Particle Physics* **41**, 055201 (2014).
- [45] W.-C. Chen and J. Piekarewicz, *Physics Letters B* **748**, 284 (2015).
- [46] J. W. Negele, *Phys. Rev. C* **1**, 1260 (1970).
- [47] M. Del Estal, M. Centelles, X. Viñas, and S. K. Patra, *Phys. Rev. C* **63**, 024314 (2001).
- [48] M. Del Estal, M. Centelles, X. Viñas, and S. K. Patra, *Phys. Rev. C* **63**, 044321 (2001), arXiv:nucl-th/0101065 [nucl-th].
- [49] Y. Gambhir, P. Ring, and A. Thimet, *Annals of Physics* **198**, 132 (1990).
- [50] Y. Sugahara and H. Toki, *Nuclear Physics A* **579**, 557 (1994).
- [51] J. Dobaczewski, H. Flocard, and J. Treiner, *Nuclear Physics A* **422**, 103 (1984).
- [52] E. Chabanat, P. Bonche, P. Haensel, J. Meyer, and R. Schaeffer, *Nuclear Physics A* **635**, 231 (1998).
- [53] T. Sil, S. K. Patra, B. K. Sharma, M. Centelles, and X. Viñas, *Phys. Rev. C* **69**, 044315 (2004).
- [54] P. B. Demorest, T. Pennucci, S. M. Ransom, M. S. E. Roberts, and J. W. T. Hessels, *Nature* **467**, 10811083 (2010), arXiv:1010.5788 [astro-ph.HE].
- [55] J. Walecka, *Ann. Phys.* **83**, 491 (1974).
- [56] H. C. Das, A. Kumar, B. Kumar, *et al.*, *MNRAS* **495**, 4893 (2020), arXiv:2002.00594 [nucl-th].
- [57] C. J. Horowitz, E. F. Brown, Y. Kim, *et al.*, *Journal of Physics G: Nuclear and Particle Physics* **41**, 093001 (2014), arXiv:1401.5839 [nucl-th].
- [58] M. Baldo and G. Burgio, *Progress in Particle and Nuclear Physics* **91**, 203258 (2016), arXiv:1606.08838 [nucl-th].
- [59] B.-A. Li and X. Han, *Physics Letters B* **727**, 276 (2013), arXiv:1304.3368 [nucl-th].
- [60] P. Danielewicz, R. Lacey, and W. G. Lynch, *Science* **298**, 1592 (2002).
- [61] B.-A. Li, P. G. Krastev, D.-H. Wen, and N.-B. Zhang, *EPJ A* **55** (2019), 10.1140/epja/i2019-12780-8, arXiv:1905.13175 [nucl-th].
- [62] T. Matsui, *Nucl. Phys. A* **370**, 365 (1981).
- [63] S. Kubis and M. Kutschera, *Phys. Lett. B* **399**, 191195 (1997).
- [64] W.-C. Chen and J. Piekarewicz, *Phys. Rev. C* **90**, 044305 (2014), arXiv:1408.4159 [nucl-th].
- [65] H. A. Bethe, *Annual Review of Nuclear Science* **21**, 93 (1971).
- [66] P. Danielewicz and J. Lee, *Nucl. Phys. A* **922**, 1 (2014), arXiv:1307.4130 [nucl-th].
- [67] J. Zimmerman, Z. Carson, K. Schumacher, A. W. Steiner, and K. Yagi, (2020), arXiv:2002.03210 [astro-ph.HE].
- [68] G. Colò, U. Garg, and H. Sagawa, *EPJ A* **50**, 26 (2014), arXiv:1309.1572 [nucl-th].
- [69] J. R. Stone, N. J. Stone, and S. A. Moszkowski, *Phys. Rev. C* **89**, 044316 (2014).
- [70] J. M. Pearson, N. Chamel, and S. Goriely, *Phys. Rev. C* **82**, 037301 (2010), arXiv:1009.3816 [nucl-th].
- [71] T. Li, U. Garg, Y. Liu, *et al.*, *Phys. Rev. C* **81**, 034309 (2010), arXiv:1002.0896 [nucl-ex].
- [72] M. Wang, G. Audi, A. Wapstra, *et al.*, *Chinese Physics C* **36**, 1603 (2012).
- [73] I. Angeli and K. Marinova, *Atomic Data and Nuclear Data Tables* **99**, 69 (2013).
- [74] S. Abrahamyan *et al.* (PREX Collaboration), *Phys. Rev. Lett.* **108**, 112502 (2012).
- [75] A. Trzcirńska, J. Jastrzębski, P. Lubiński, *et al.*, *Phys. Rev. Lett.* **87**, 082501 (2001).
- [76] J. Zenihiro, H. Sakaguchi, T. Murakami, *et al.*, *Phys. Rev. C* **82**, 044611 (2010).
- [77] D. Vautherin and D. M. Brink, *Phys. Rev. C* **5**, 626 (1972).
- [78] P. Miller, A. Sierk, T. Ichikawa, and H. Sagawa, *Atomic Data and Nuclear Data Tables* **109-110**, 1 (2016), arXiv:1508.06294 [nucl-th].
- [79] K. Rutz, M. Bender, T. Bürvenich, *et al.*, *Phys. Rev. C* **56**, 238 (1997), arXiv:9610032 [nucl-th].
- [80] R. K. Gupta, S. K. Patra, and W. Greiner, *Modern Physics Letters A* **12**, 1727 (1997).
- [81] S. K. Patra, C.-L. Wu, C. R. Praharaj, and R. K. Gupta, *Nuclear Physics A* **651**, 117 (1999).
- [82] M. S. Mehta, H. Kaur, B. Kumar, and S. K. Patra, *Phys. Rev. C* **92**, 054305 (2015).
- [83] M. Bhuyan and S. K. Patra, *Mod. Phys. Lett. A* **27**, 1250173 (2012), arXiv:1111.6487 [nucl-th].
- [84] K. Hebeler, J. M. Lattimer, C. J. Pethick, and A. Schwenk, *The Astrophysical Journal* **773**, 11 (2013), arXiv:1303.4662 [astro-ph.SR].
- [85] A. Gezerlis and J. Carlson, *Phys. Rev. C* **81**, 025803 (2010), arXiv:0911.3907 [nucl-th].
- [86] M. Baldo and C. Maieron, *Phys. Rev. C* **77**, 015801 (2008), arXiv:0712.2662 [nucl-th].
- [87] B. Friedman and V. Pandharipande, *Nuclear Physics A* **361**, 502 (1981).
- [88] S. Gandolfi, A. Y. Illarionov, S. Fantoni, F. Pederiva, and K. E. Schmidt, *Phys. Rev. Lett.* **101**, 132501 (2008), arXiv:0805.2513 [nucl-th].
- [89] M. B. Tsang, Y. Zhang, P. Danielewicz, *et al.*, *Phys. Rev. Lett.* **102**, 122701 (2009), arXiv:0811.3107 [nucl-ex].
- [90] M. B. Tsang *et al.*, *IJMPA* **19**, 1631 (2010), arXiv:0811.3107 [nucl-ex].
- [91] P. Russotto *et al.*, *Phys. Rev. C* **94**, 034608 (2016), arXiv:1608.04332 [nucl-ex].
- [92] C. Dorso, G. Frank, and J. Lpez, *Nuclear Physics A* **984**, 77 (2019), arXiv:1809.03370 [nucl-th].
- [93] J. M. Lattimer, *Nuclear Physics A* **928**, 276 (2014).

- [94] S. Gandolfi and A. W. Steiner, *Journal of Physics: Conference Series* **665**, 012063 (2016).
- [95] N. K. Glendenning, *Compact stars: Nuclear physics, particle physics, and general relativity* (Springer-Verlag New York, 1997).
- [96] B. K. Sharma, M. Centelles, X. Viñas, M. Baldo, and G. F. Burgio, *A&A* **584**, A103 (2015), arXiv:1506.00375 [nucl-th].
- [97] T. Hinderer, B. D. Lackey, R. N. Lang, and J. S. Read, *Phys. Rev. D* **81**, 123016 (2010), arXiv:0911.3535 [astro-ph.HE].
- [98] B. Kumar, S. K. Biswal, and S. K. Patra, *Phys. Rev. C* **95**, 015801 (2017), arXiv:1609.08863 [nucl-th].
- [99] E. E. Flanagan and T. Hinderer, *Phys. Rev. D* **77**, 021502 (2008), arXiv:0709.1915 [astro-ph].
- [100] T. Hinderer, *The Astrophysical Journal* **677**, 1216 (2008), arXiv:0711.2420 [astro-ph].
- [101] R. C. Tolman, *Phys. Rev.* **55**, 364 (1939).
- [102] J. R. Oppenheimer and G. M. Volkoff, *Phys. Rev.* **55**, 374 (1939).
- [103] J. Antoniadis, P. C. C. Freire, *et al.*, *Science* **340** (2013), 10.1126/science.1233232, arXiv:1304.6875 [astro-ph.HE].
- [104] L. Rezzolla, E. R. Most, and L. R. Weih, *The Astrophysical Journal* **852**, L25 (2018), arXiv:1711.00314 [astro-ph.HE].
- [105] L. D. Miller and A. E. S. Green, *Phys. Rev. C* **5**, 241 (1972).
- [106] J. M. Lattimer and M. Prakash, *Physics Reports* **333-334**, 121146 (2000), arXiv:astro-ph/0002203 [astro-ph].
- [107] P. G. Krastev, B. Li, and A. Worley, *APJ* **676**, 11701177 (2008), arXiv:0709.3621 [astro-ph].
- [108] P. Landry and B. Kumar, *APJ* **868**, L22 (2018), arXiv:1807.04727 [gr-qc].
- [109] B. Kumar and P. Landry, *Phys. Rev. D* **99**, 123026 (2019), arXiv:1902.04557 [gr-qc].